Available online at www.sciencedirect.com
SCIENCE DIRECT
Journal of Magnetic Resonance 179 (2006) 29–37
JMR Journal of Magnetic Resonance
www.elsevier.com/locate/jmr

Single-ion and molecular contributions to the zero-field splitting in an iron(III)-oxo dimer studied by single crystal W-band EPR

Peter ter Heerdt [a], Mariana Stefan [b], Etienne Goovaerts [a,*], Andrea Caneschi [c], Andrea Cornia [d]

[a] Physics Department—CDE, University of Antwerp, Universiteitsplein 1, B-2610 Antwerpen (Wilrijk), Belgium
[b] National Institute for Materials Physics, P.O. Box MG-7, Magurele-Bucuresti 077125, Romania
[c] Department of Chemistry, INSTM and University of Florence, I-50019 Sesto Fiorentina (Fi), Italy
[d] Department of Chemistry, INSTM and University of Modena and Reggio Emilia, Via G. Campi 183, I-41100 Modena, Italy

Received 14 September 2005; revised 24 October 2005
Available online 1 December 2005

Abstract

Detailed knowledge of the type and strength of pair interactions between high-spin metal ions is paramount to the understanding and design of molecular magnetic materials. In this work, the anisotropic magnetic interactions in a β-diketonate-alkoxide iron(III) dimer compound, $[Fe_2(OCH_3)_2(dbm)_4$, Hdbm = dibenzoylmethane] (Fe2) have been investigated by single crystal electron paramagnetic resonance (EPR) in the W-band (at 95 GHz). The diamagnetic substitution method was employed using the isomorphous gallium(III)-based compound doped with iron(III) to produce Ga–Fe dimers (GaFe). The single-ion zero-field splitting (ZFS) tensor could be separately determined in GaFe with the iron ion in a local environment quasi-identical to the one in Fe2. Its principal directions are found to point in arbitrary directions, uncorrelated with the Fe–O bonds. The Fe2 EPR spectra consist of transitions within the lowest multiplet states $S = 1, 2, 3$, which were analyzed using the full spin Hamiltonian description of an exchange coupled pair of $s = 5/2$ spins. The anisotropic spin–spin interaction tensor of Fe2 possesses a principal axis close to the Fe–Fe direction and was shown to arise both from through-space (dipolar) and through-bond (anisotropic exchange) contributions. The latter involves an rhombic component $J_E = (J_X - J_Y)/2 \approx 0.093$ cm^{-1} of magnitude comparable to the dipolar interaction, and even to the rhombic part of the single-ion ZFS ($E = 0.097$ cm^{-1}). Our results show that the anisotropic exchange, usually neglected for *S*-type ions, is significant for the anisotropic interactions in exchange-coupled iron(III) clusters, including the Fe_4 and Fe_8 families of single-molecule magnets and the antiferromagnetic iron wheels.

Keywords: Iron; Dimer; Oxo-ligands; Magnetic properties; EPR-spectroscopy

1. Introduction

Magnetic properties of molecules and the engineering of molecular magnetic materials are the subjects of the growing field of Molecular Magnetism [1]. In particular, molecular clusters of transition metal ions have been under intense investigation in the past decade as nanoscale magnetic units [2–4]. Great attention has been devoted to a number of iron [5–8], manganese [9,10], nickel [11,12], and cobalt [13] clusters which show magnetic hysteresis below a characteristic, material-dependent temperature [14–17]. Such *single molecule magnets* (SMMs) are currently regarded as candidates for data storage at the molecular level [18] thus holding the promise for a giant leap in the miniaturisation of memory devices. Also, due to their nanoscale size they show interesting quantum mechanical (QM) features such as quantum tunnelling of the magnetization [19–22]. Owing to these intrinsic QM properties, they were proposed to serve as the basic elements (or "*qubits*") of quantum computers [23]. Cyclic antiferromagnetically (AFM)-coupled clusters (or "*magnetic wheels*") [24–26] have also been extensively investigated as model systems for the observation of macroscopic quantum

* Corresponding author. Fax: +32 3 820 2245.
E-mail address: Etienne.Goovaerts@ua.ac.be (E. Goovaerts).

1090-7807/$ - see front matter © 2005 Elsevier Inc. All rights reserved.
doi:10.1016/j.jmr.2005.10.016

coherence [24a] and, more recently, as qubits for quantum computation [24b].

To design and synthesize new molecular clusters with enhanced magnetic properties, a deep understanding and control of their magnetic anisotropy is mandatory [27]. Molecular magnetic anisotropy in the ground and excited spin states has been measured using a variety of techniques, including electron spin resonance (EPR), Inelastic neutron scattering and torque magnetometry [6,14,15,27–29]. However, only in few cases the origin of magnetic anisotropy was studied in detail [30], particularly in the case of weakly anisotropic metal ions such as high-spin iron(III) ($s = 5/2$), where single-ion and spin–spin terms are expected to have a comparable magnitude. Single-ion terms can be estimated using the diamagnetic substitution approach, i.e., by investigating doped samples of diamagnetic analogs, when available [31], as reported in the case of a hexairon(III) ring [27]. However, further analysis of spin–spin terms with precise separation of dipolar (through-space) and anisotropic-exchange (through-bond) contributions is often impossible in high-nuclearity spin clusters.

The investigation of simpler model systems like iron(III)-oxo dimers would be of great help in the optimal design and control of iron(III)-based SMMs and magnetic wheels. Surprisingly, a preliminary literature survey showed that, although a number of iron(III) dimers have been previously studied, the origin of their anisotropic magnetic interactions was rarely ascertained [30].

The compound studied in this work is the AFM-coupled iron(III)-alkoxo dimer $[Fe_2(OCH_3)_2(dbm)_4]$, with Hdbm = dibenzoylmethane (notation: Fe2), which forms an ideal model to accurately investigate the origin of the magnetic anisotropy and to precisely separate single-ion from spin–spin interactions. An isomorphous gallium(III) analog (Ga2) is in fact available which can be doped with iron(III) ions, affording mixed-metal complexes diluted in a diamagnetic crystalline matrix (GaFe). According to a previous investigation by high-frequency EPR on a microcrystalline sample, the single-ion anisotropy in GaFe is of the hard-axis type, with a small rhombic component [$D = 0.770(3)$ cm^{-1}, $E = 0.090(3)$ cm^{-1}] [27]. However, the orientation of the ZFS tensor relative to the crystallographic axes could not be determined. We have now fully characterized the ZFS tensor of GaFe by single-crystal EPR experiments in the W-band (~95 GHz) and have performed variable-temperature EPR measurements on single crystals of Fe2. Our combined studies provide a consistent picture of the different contributions to magnetic anisotropy in Fe2 and clearly reveal the anisotropic character of spin–spin interactions.

2. Results and discussion

2.1. Diamagnetic substitution approach

The structure of Fe2, which crystallizes in triclinic space group $P\bar{1}$ ($Z = 1$), is depicted in Fig. 1. This low symmetry structure contains only one molecule per unit cell. The two iron(III) ions are related by an inversion center and are coordinated by two bridging methoxides and four β-diketonate ligands. Compound Ga2 has very similar lattice parameters and a nearly identical molecular structure. Corresponding bond lengths and angles agree within 0.047 Å and 3.5°, respectively [27], in the two compounds, lending support to the validity of the diamagnetic substitution approach. In the preparation of iron(III)-doped Ga2, a low doping level (2.0 mol% of Fe) has been chosen in order to minimize dipolar interactions between the paramagnetic ions and to have a very small probability of substitution of both Ga(III) ions in the same molecule. Modelling isomorphic substitutions as independent events [27], the percentage of FeFe species is calculated to be 0.04% only, while about 4% of the molecules consist of GaFe pairs. Notice that the two possible sites for iron substitution in the Ga2 molecule are related by inversion symmetry, and are thus structurally and magnetically equivalent.

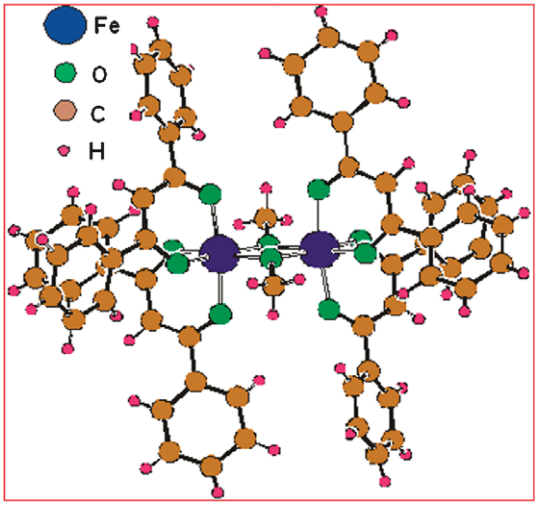

Fig. 1. Structure of the Fe2 compound.

The analysis of single-ion and molecular contributions to the magnetic anisotropy in Fe2, to be illustrated in Sections 2.2 and 2.3, starts from an accurate determination of the single-ion ZFS-tensor of the Fe(III) ion ($s = 5/2$) in iron(III)-doped Ga2 (in Section 2.2). In light of the similar single-ion anisotropies expected in Fe2 and GaFe, the results will represent an excellent starting point to analyze single-crystal EPR spectra of Fe2. In a second step (Section 2.3), the magnetic anisotropy of the Fe2 dimer will be fully analyzed in terms of single-ion and spin–spin contributions.

2.2. Single-ion anisotropy in the mixed GaFe molecule

In single crystals of iron(III)-doped Ga2, angular-dependent EPR measurements were performed at room temperature (RT) over a range of 180° in the three mutually orthogonal planes of the (xyz) reference system. The xz-plane was chosen to coincide with the ac crystallographic plane, with x along the a axis. The EPR spectra, shown

in Fig. 2 for the magnetic field along three reference axes, consist of relatively narrow resonance lines ($\Delta B \approx 8$ mT) which were identified as the allowed ($\Delta m_S = \pm 1$) and forbidden transitions of an Fe(III) $s = 5/2$ center. The angular dependence pattern possesses only 180° symmetry (see Fig. 3), as expected from the low symmetry of the ionic site. The angular dependence in the *ac* plane was also measured at 15 K over a 140° range, with identical mounting of the same sample, which resulted in relatively small shifts of the positions and separations of the resonance lines, corresponding to small variations in D (of $\sim$0.05 cm $^{-1}$) and E (of $\sim$0.012 cm $^{-1}$) and in the principal orientations (<5°) with temperature.

The line positions could be accurately fitted with the regular spin Hamiltonian [32]

$$H_{\mathrm{GaFe}} = \mu_B B \cdot g \cdot s + s \cdot D_{\mathrm{SI}} \cdot s \qquad (1)$$

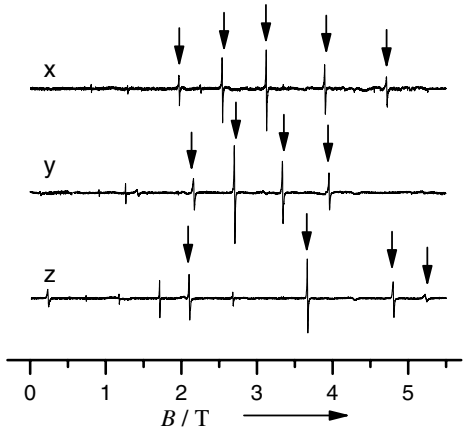

Fig. 2. W-band spectra of GaFe in single crystals of the iron doped Ga2 compound, with the magnetic field along the axes of the orthogonal reference frame, at room temperature. The arrows indicate allowed transitions.

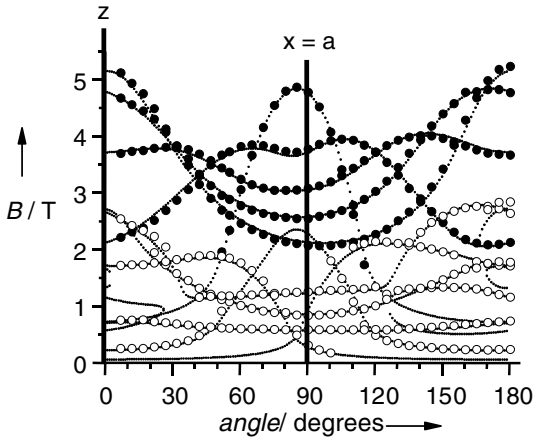

Fig. 3. Angular dependence of the GaFe resonance lines in the $xz = ac$ plane, measured at room temperature. The solid and open black circles indicate the allowed and forbidden transitions, respectively, and the dotted lines represent the calculated field positions.

with $s = 5/2$ for Fe(III). The first term in (1) describes the Zeeman interaction, while the second term represents the ZFS of the paramagnetic Fe(III) center and contains the single-ion ZFS interaction tensor D_{SI}. The two possible sites for Fe(III) in the GaFe dimer, related by inversion symmetry, are magnetically equivalent and thus described by the same Hamiltonian. There are no symmetry-related constraints on the single ion tensor $\mathrm{D_{SI}}$, which can be a general symmetric traceless tensor. In the EPR analysis, we have adopted an isotropic g-value, $g = 2.000$. This is not in contradiction with the very small g-anisotropy ($g_{\perp,\mathrm{powder}} = 2.003$, $g_{//,\mathrm{powder}} = 2.000$) determined from previous EPR measurements at 525 GHz [27] on powder samples: extensive testing during the analysis of our data showed that such a small g-anisotropy could not be resolved in our W-band EPR (95 GHz) measurements.

The following D-tensor, expressed in the orthogonal (xyz) reference frame, was derived from fitting the experimental data at RT in the three orthogonal planes

$$D_{\mathrm{SI}} = \begin{pmatrix} -0.221 & -0.098 & -0.030 \\ -0.098 & -0.181 & 0.250 \\ -0.030 & 0.250 & 0.402 \end{pmatrix} \mathrm{cm}^{-1} \qquad (2)$$

Error analysis yielded maximum standard deviations of 0.002 cm^{-1} for the elements of D_{SI}. The angular dependence calculated with these parameters fits the experimental data for both the allowed and forbidden transitions very well, as one can see in Fig. 3, where the angular variation of the Fe(III) transitions in the crystalline *ac*-plane is displayed (other planes in the Supporting information). Diagonalization of this tensor yields the principal directions and values D_X, D_Y, and D_Z of the ZFS interaction in the GaFe molecule. The principal axes of D_{SI}, defined by the direction cosines $X_D = (-0.796,\ 0.536,\ -0.279)$, $Y_D = (-0.598,\ -0.766,\ 0.236)$, $Z_D = (-0.087,\ 0.355,\ 0.931)$ with respect to the chosen (xyz) reference system, are shown in Fig. 4 and seem to have no clear correlation with the Fe–O bonds. The corresponding ZFS parameters are $D = 3/2D_Z = 0.749(4)$ cm^{-1} and $E = 1/2(D_X - D_Y) = 0.085(2)$ cm^{-1} (the number in brackets is the estimated accuracy in the last digit), in good agreement with the values $D_{\mathrm{powder}} = 0.77$ cm^{-1} and $E_{\mathrm{powder}} = 0.09$ cm^{-1} obtained from measurements on microcrystalline samples at 525 GHz [27].

2.3. Spin–spin interactions in the Fe(III)-oxo-dimer

Unlike the case of GaFe, where the Fe(III) spectra are perfectly visible at RT due to the long spin–lattice relaxation time characteristic for S-type ions, the EPR-spectra of Fe2 single crystals are excessively broadened at temperatures above 150 K. Below this temperature, an interesting temperature variation is observed. As shown in Fig. 5 for temperatures from 5 to 50 K, new groups of lines emerge and gain intensity with increasing temperature. From temperature-dependent magnetic susceptibility measurements [33], using the Heisenberg interaction, J_0

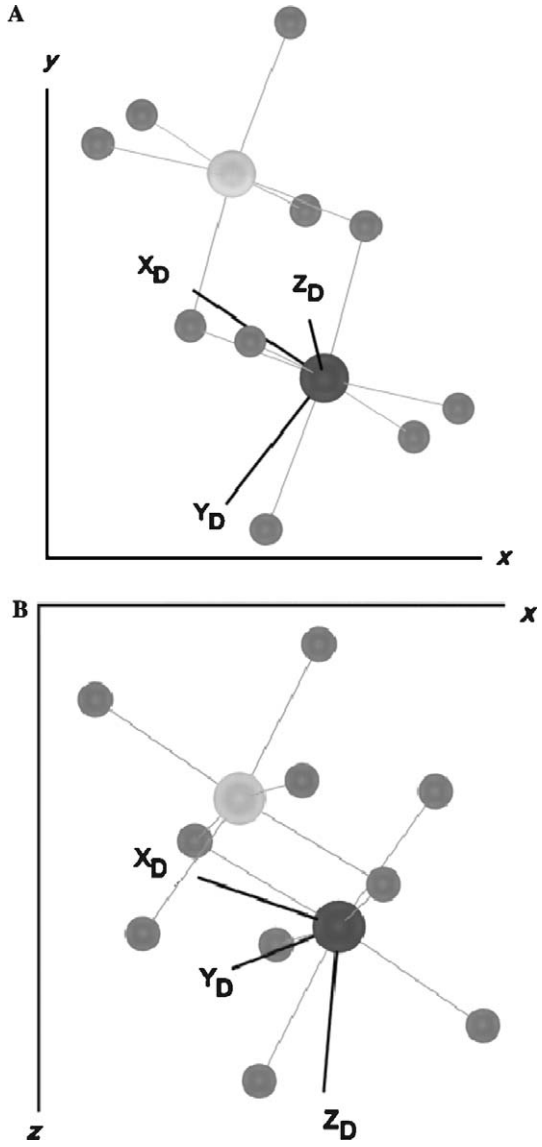

Fig. 4. Drawing of the principal directions of the single-ion ZFS tensor D_{SI} of Fe(III) in GaFe viewed along the (A) z and (B) y direction. For simplicity only the neighboring oxygen atoms are shown together with the two metal ions.

$s_1 \cdot s_2$, an AFM exchange coupling with $J_0 = 15.4\ \mathrm{cm}^{-1}$ between the two $s = 5/2$ spins was determined, leading to an $S = 0$ ground state. The temperature dependence of the EPR line intensities is consistent with thermal population of the different paramagnetic multiplets $S = 1$, 2, and 3, indicated in Fig. 5. In the $T = 50$ K spectrum a number of weaker lines appear, which are identified as transitions within the higher $S = 4$ and 5 multiplets. Indeed, the isotropic exchange is large relative to the anisotropic interactions and the Zeeman terms, and therefore the projection of the spin Hamiltonian within each of the multiplets is a reasonable lowest-order approximation. The observation of EPR lines from the different multiplets is only possible when the intra- and intermultiplet spin relaxation is sufficiently slow.

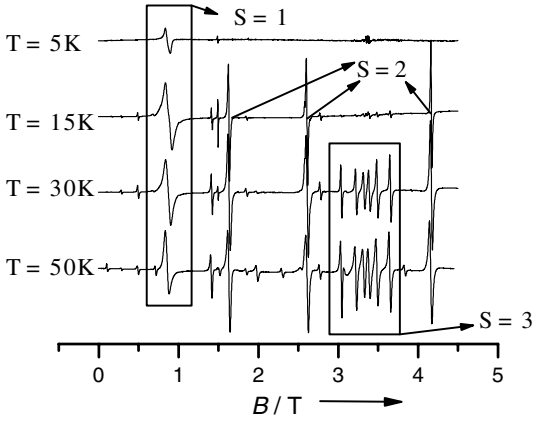

Fig. 5. Temperature-dependent EPR measurements of the Fe2 dimer from 5 K up to 50 K probing the occupation of the different spin multiplets with increasing temperature. This particular orientation in the *bc* crystalline plane, at ≈20° from the c-axis, was chosen because the groups of lines belonging to different multiplets were well defined and separated.

In Fig. 5, a particular orientation in the *bc* crystalline plane, at ≈20° from the *c*-axis, was chosen for which the lines belonging to different multiplets were well defined and separated. This was not the case in general: for other orientations a splitting in two equally intense components separated by up to 100 mT was observed for almost every EPR line of the dimer (see Supporting information)). Up to now, the exact origin of this splitting is not elucidated. A possible explanation is the presence of two isomers differing by the conformation of the outer ligands of the molecule, which could result in slightly different sets of interaction parameters and thus different resonance fields [28], but this could not been confirmed by X-ray diffraction. A phase transition below RT, inducing inequivalence between neighboring Fe2 molecules (e.g., doubling of the unit cell), forms an attractive alternative.

The Fe2 EPR spectra could be accurately described on the basis of the spin Hamiltonian [34]

$$H_{\mathrm{Fe2}} = \mu_{\mathrm{B}} B \cdot g \cdot S + s_1 \cdot D'_{\mathrm{SI}} \cdot s_1 + s_2 \cdot D'_{SI} \cdot s_2 + J_0 s_1 \cdot s_2 + s_1 \cdot J \cdot s_2, \quad (3)$$

where $s_1 = s_2 = 5/2$, $S = s_1 + s_2$, and D'_{SI} is the single ion ZFS tensor of the Fe(III) ion in the dimer. The g-matrix and single ion ZFS-tensor are common to the two iron ions because their sites are related by inversion symmetry. Besides the single-ion terms the interactions between the spins were taken into account, i.e., the isotropic exchange, described by J_0 ($=15.4\ \mathrm{cm}^{-1}$) [33], and the anisotropic spin–spin interaction. The latter is described by the symmetric traceless tensor J and in principle contains both through-space (dipolar) and through-bond (anisotropic exchange) contributions. In general, an antisymmetric part could occur in the spin–spin interactions but in this case it is absent because of the presence of inversion symmetry within the molecule. As in the case of GaFe, an isotropic g-value $g = 2.000$ was employed in the further analysis, after having checked that the influence of the

expected small g-shifts on the W-band spectra is negligible.

In a first approach, an attempt was made to analyze the data in the framework of the strong exchange limit. A separate analysis was performed for the $S = 1$ and the $S = 2$ multiplets using the projected spin Hamiltonians

$$H_{\mathrm{Fe2},S} = \mu_B B \cdot g \cdot S + S \cdot d_S \cdot S + J_0[S(S+1) - 35/4], \quad (4a)$$

where

$$d_S = 2\alpha_1 D'_{\mathrm{SI}} + \alpha_{12} J \quad (4b)$$

is the projected ZFS tensor and α_1 and α_{12} are weight factors listed in [34]. For the combination of two $s = 5/2$ spins they assume the respective values $-16/5$ and $37/10$ for $S = 1$, $-10/21$ and $41/42$ for $S = 2$, and $-1/45$ and $47/90$ for $S = 3$. These coefficients strongly decrease from $S = 1$ to 3 corresponding to decreasing magnitudes of the line splittings as can be seen in Fig. 5. From the two d_S tensors for $S = 1$ and 2, one could in principle derive the tensors D'_{SI} and J defined in Eq. (3) because their relative weight is different in the two multiplets. The apparent advantage of this approach is the lower dimensionality $(2S + 1)$ of the space in which the Hamiltonian has to be diagonalized, compared to the dimension $(2s_1 + 1)(2s_1 + 1) = 36$ of the initial product space. In each multiplet, 5 independent parameters occur in the projected ZFS tensor. Within each of the $S = 1$ and $S = 2$ multiplets it was possible to derive ZFS tensors $d_{S=1}$ and $d_{S=2}$ which accurately described the angular variation patterns of the respective resonance lines. But an important drawback occurred in this approach. With D'_{SI} known from the GaFe experiments it was not possible to determine a unique spin–spin tensor J, i.e., there was no proper correlation between $d_{S=1}$ and $d_{S=2}$ through relation (4b). Several effects probably contribute to this failure of the projection model. First, only few allowed transitions are observed for the $S = 1$ triplet compared to the $S = 2$ quintet and moreover no forbidden transitions were experimentally observed within the triplet. The limited amount of data available for $S = 1$ for the determination of a fairly large number of unknown parameters may have lead to larger errors in the determination of $d_{S=1}$. Second, the resulting spin–spin tensor must be derived from relation (4b) and results essentially from a weighed difference between two tensors and such a numerical operation typically amplifies the relative errors on the resulting parameters. Third, the isotropic exchange is not large enough compared to other interactions, that the errors introduced by projection into the multiplets (neglecting the off-diagonal matrix elements between multiplets) can be safely neglected: they may contribute as well to the failure of this approach. Along some field directions we have found differences of several hundred millitesla between the line positions of Fe2 calculated with the projected Hamiltonian approach and the full Hamiltonian approach (as described below), respectively (see also Supporting information).

Therefore, we decided to perform the EPR analysis by diagonalization of the full Hamiltonian (3) in the product space of spin states. In this approach the data from different multiplets are fitted simultaneously, resulting in a more reliable and consistent determination of the tensors D'_{SI} and J.

Higher-order contributions were not included in Hamiltonian (3). Liviotti et al. [35a,35b] demonstrated that the experimentally observed higher-order ZFS terms in other members of the Fe(III)-oxo family (like Fe4 and Fe8) were well explained by the mechanism of "*S-mixing*" which admixes the nearest excited S-multiplets into the ground state multiplet. Our analysis however was performed in the full product space of spins. In this way, one automatically incorporates off-diagonal matrix elements between all S-multiplets. The only possible higher-order terms left are the single-ion contributions. In view of the arguments in [35a,35b], they are expected to be negligible. Additional tests on the presence of higher-order single-ion ZFS terms revealed no significant changes in the simulations and confirmed our expectations.

The angular dependence of the Fe2 spectra was measured in the crystallographic *ac*, *bc*, and *ab* planes at 15 K, as depicted in Fig. 6A for the $xz = ac$-plane (other

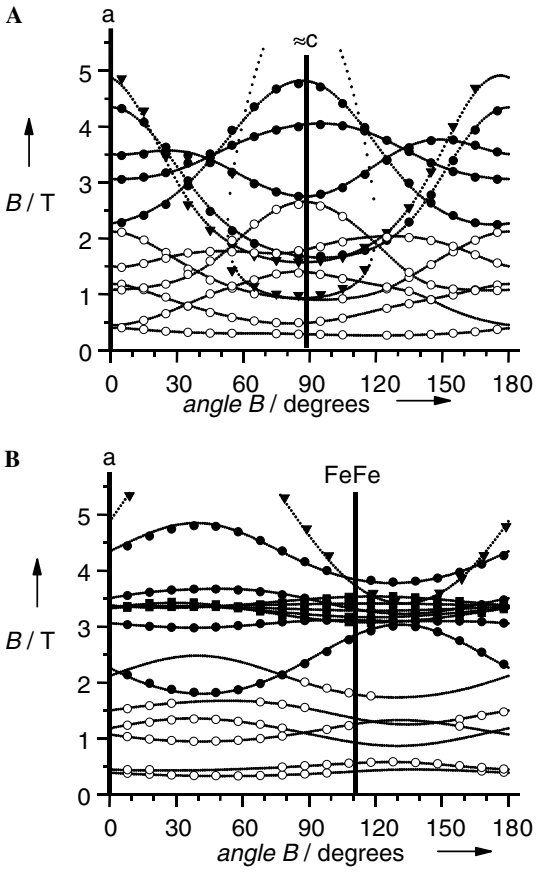

Fig. 6. Angular variation of the Fe2 resonance lines: (A) in the $xz = ac$ plane at $T = 15$ K, and (B) in the plane containing the a axis and the Fe–Fe direction at $T = 30$ K. The solid triangles indicate the $S = 1$ allowed transitions, the solid circles the $S = 2$ allowed transitions, the open circles the $S = 2$ forbidden transitions and in (B) the solid squares represent the $S = 3$ allowed transitions. The dotted lines show the field positions calculated using the full Hamiltonian (3).

planes in Supporting information) in which allowed and forbidden resonances of both the $S = 1$ and 2 multiplets are shown. Relying on the diamagnetic substitution method, the single-ion ZFS-tensor D'_{SI} was first identified with the D_{SI} tensor of GaFe (Eq. (2)), for simultaneous fitting of all the available transition fields in the three planes pertaining to the $S = 1$ and 2 levels. Although it was possible to qualitatively reproduce the angular variations of the resonance fields, unacceptable discrepancies were found between experimental and calculated line positions.

More accurate fitting of the experimental data was possible when the assumption $D'_{SI} = D_{SI}$ was relaxed and the two tensors describing single-ion and spin–spin interactions were both varied. In this problem, one deals with 10 independent parameters, i.e., the elements of two symmetrical traceless tensors, compared to only 5 in the GaFe case. To impose further constraints on this large number of parameters, additional measurements of the $S = 1, 2$ as well as $S = 3$ transitions (simultaneously observable at $T = 30$ K) were performed in an accurately oriented plane (see Section 4) containing both the $x = a$ axis and the Fe–Fe direction, i.e., the symmetry axis of the dipolar interaction. In Fig. 6, the experimental data and the best fit curves are shown for the angular variations in the *ac* and *a*–Fe-Fe planes (other planes in Supporting information), calculated with the following numerical values of the interaction tensors:

$$D'_{SI} = \begin{pmatrix} -0.242 & -0.077 & 0.063 \\ -0.077 & -0.120 & 0.290 \\ 0.063 & 0.290 & 0.362 \end{pmatrix} \text{cm}^{-1} \quad \text{and}$$
$$J = \begin{pmatrix} -0.030 & 0.060 & 0.038 \\ 0.060 & 0.000 & 0.096 \\ 0.038 & 0.096 & 0.030 \end{pmatrix} \text{cm}^{-1}. \tag{4c}$$

Error analysis yielded maximum standard deviations of 0.003 and 0.004 cm^{-1} for the elements of the D'_{SI} and J tensors, respectively.

Projection in the different multiplets, using Eq. (4b), yields the following effective axial and rhombic ZFS parameters from the principal values of d_S:

for $S = 1$: $D = -4.248\ \text{cm}^{-1}$ $E = 0.761\ \text{cm}^{-1}$,

for $S = 2$: $D = -0.575\ \text{cm}^{-1}$ $E = 0.132\ \text{cm}^{-1}$,

for $S = 3$: $D = 0.092\ \text{cm}^{-1}$ $E = 0.011\ \text{cm}^{-1}$,

which shows the large negative D-value for the triplet state, and strongly decreasing values for the quintet and septet, corresponding to the decreasing line splittings (see Fig. 5). In different multiplets, the d_S tensor possesses different principal directions, because the single-ion and spin–spin contributions possess different main axes.

The D'_{SI} tensor of Fe2 is very similar to D_{SI} (see Eq. (2)) of GaFe, which is consistent with the assumptions of the diamagnetic substitution method. Evidently, the knowledge of the ZFS tensor of GaFe has been an invaluable starting point for the analysis of the anisotropic interactions in Fe2. For the ZFS parameters, nearly identical values $D_{SI}(\text{Fe2}) = 0.749(6)\ \text{cm}^{-1}$ and $E_{SI}(\text{Fe2}) = 0.097(3)\ \text{cm}^{-1}$ are found as from the GaFe analysis (Section 2.2). The principal directions $X_{D'} = (-0.729, 0.630, -0.266)$, $Y_{D'} = (-0.683, -0.652, 0.328)$, and $Z_{D'} = (0.033, 0.421, 0.906)$ deviate from the corresponding ones of D_{SI} by less than 10°. They are visualized in Fig. 7, and again point in general directions, not obviously correlated to coordination bonds or interatomic vectors.

The difference between D_{SI} and D'_{SI} can be attributed to different factors: (i) the most important one is probably the change in the ZFS tensor from RT to low temperatures as indicated by the measurements for GaFe; (ii) small differences in chemical environment of the iron ion in the GaFe and Fe2 molecules; (iii) errors expected mainly from the

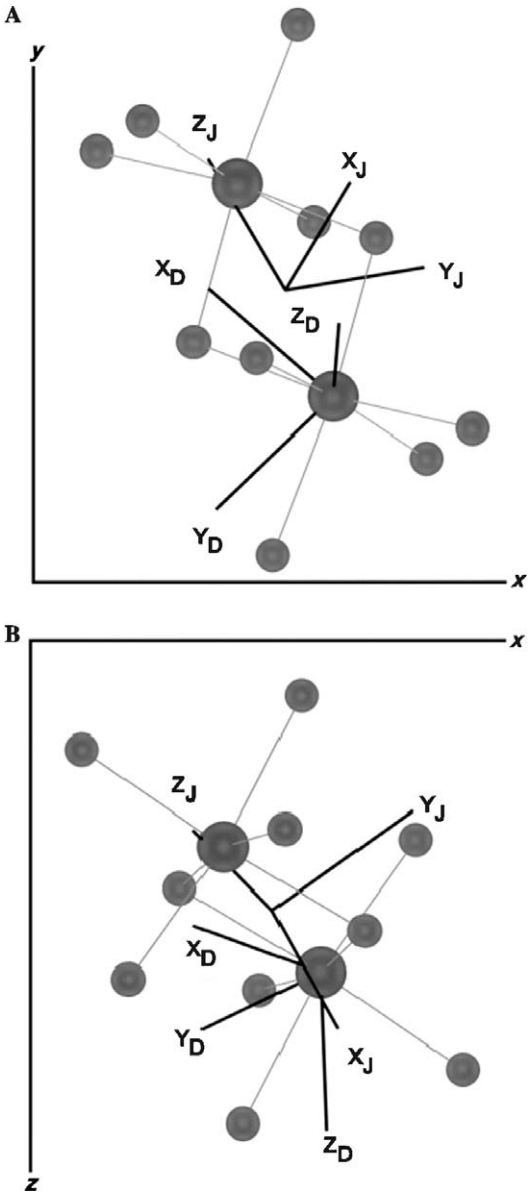

Fig. 7. Drawing of the principal directions of the single-ion ZFS tensor D'_{SI} and the spin–spin interaction tensor J with respect to the Fe2 molecule, showing only the iron ions and neighboring oxygen atoms. (A) and (B) are views along the z and y directions, respectively.

experimental uncertainties in the orientation of the various planes for the EPR measurements.

The principal directions $X_J = (0.378,\ 0.629,\ 0.679)$ $Y_J = (0.809,\ 0.132,\ -0.573)$, and $Z_J = (-0.450,\ 0.766,\ -0.458)$ of the spin–spin interaction tensor J are shown in Fig. 7 as a reference frame at midpoint between the two iron(III) ions. The Z_J direction lies very close (5.5°) to the expected symmetry axis of the dipolar interaction, the Fe–Fe direction $(-0.363,\ 0.806,\ -0.468)$. The small deviation may well fall within the confidence region for the determination of the principal directions from the fitting procedure. However, inspection of the principal values

$$J_X = 0.140(5)\ \mathrm{cm}^{-1},\ J_Y = -0.047(6)\ \mathrm{cm}^{-1},\ \text{and}$$
$$J_Z = -0.093(5)\ \mathrm{cm}^{-1},$$

corresponding to an axial and rhombic component

$$J_D = 3/2\ J_Z = -0.138(8)\ \mathrm{cm}^{-1} \quad \text{and}$$
$$J_E = (J_X - J_Y)/2 = 0.093(4)\ \mathrm{cm}^{-1},$$

indicates that the J tensor strongly departs from axial symmetry. Expressing J as the sum of dipolar and anisotropic exchange terms:

$$J = J_{\mathrm{dip}} + J_{\mathrm{ex}},$$

and calculating J_{dip} in the point-dipole approximation [34] one can evaluate J_{ex}. Neglecting the small deviation of Z_J from the Fe–Fe direction, the result is

$$J_{\mathrm{dip},X} = J_{\mathrm{dip},Y} = g^2\mu_B^2/R^3 = 0.059\ \mathrm{cm}^{-1} \quad \text{and}$$
$$J_{\mathrm{dip},Z} = -2g^2\mu_B^2/R^3 = -0.118\ \mathrm{cm}^{-1},$$
$$J_{\mathrm{ex},X} = 0.081\ \mathrm{cm}^{-1},\ J_{\mathrm{ex},Y} = -0.106\ \mathrm{cm}^{-1} \quad \text{and}$$
$$J_{\mathrm{ex},Z} = 0.025\ \mathrm{cm}^{-1}$$

with $g = 2.000$, μ_B is the Bohr magneton, and the interionic distance $R = 3.07$ Å at RT as determined in [33]. Lowering the temperature would reduce the distance R and thus increase the magnitude of the (negative) axial dipolar contribution, leading to a somewhat larger value for $J_{\mathrm{ex},Z}$ (e.g., contraction of the Fe–Fe distance to 2.97 Å, i.e., linear contraction of ~3% which can be considered a safe upper limit for this type of materials, would lead to $J_{\mathrm{dip},Z} = -0.130\ \mathrm{cm}^{-1}$ and $J_{\mathrm{ex},Z} = 0.037\ \mathrm{cm}^{-1}$).

As a result of the axial symmetry of J_{dip}, the rhombic part of the spin–spin interaction is entirely originating from the anisotropic exchange $J_{\mathrm{dip},E} = J_E$. Although the presented analysis heavily relies on the assumption of point magnetic dipoles, a rhombic contribution J_E to spin–spin interactions is clearly present, indicating that a significant anisotropic-exchange interaction is operative. It is much smaller than the isotropic one, $\|J_{ex}/J_o\| \approx 1/150$, but the magnitude is indeed comparable to that of the dipolar interaction, demonstrating that the anisotropic spin–spin interaction is not simply dominated by the dipolar coupling between the Fe(III) ions.

This is quite surprising considering the nature of Fe(III), an S-type ion. Indeed, many examples are found in literature, where the anisotropic exchange is neglected and only the isotropic exchange is considered [31,36,37]. In a few other cases, in particular dimers of the Cu(II), ^{2}D ion [38–40], the anisotropic exchange was considered in more detail and could be quite well described in terms of a simplified model considering the admixture of an excited state of the dimer with one ion in a higher configuration. In this description, also called the Moriya approximation, anisotropic exchange parameters of the order $(\Delta g/g)^2 J'$ are obtained, with Δg the g-shift from the free electron value and J' a matrix element of the exchange interaction between the ground state of one copper ion and the excited state of the other one. However, the g-shifts in Fe2 are extremely small (≈0.003 according to the high-frequency powder experiments [27]) and, taking the value of the isotropic exchange J_0 as an estimate of J', an anisotropic exchange interaction of the order of $10^{-4}\ \mathrm{cm}^{-1}$ would be expected, three orders of magnitude lower than observed. Our results are compatible with those of Ozarowski et al. [30] for two Fe–O–Fe dimer compounds, in which the anisotropic exchange is found to be even larger than the dipolar contributions, nearly an order of magnitude higher than for the Fe2 molecule in the present investigation. This correlates with the much higher isotropic exchange in their compounds ($J_0 \approx 200\ \mathrm{cm}^{-1}$ compared to $J_0 = 15.4\ \mathrm{cm}^{-1}$ for Fe2). These results reveal a lack of understanding of anisotropic exchange interactions in transition metal dimers of S-ions and the need for a more sophisticated calculation in these systems.

3. Conclusion

From detailed single-crystal high-frequency EPR measurements, we have investigated the origin of magnetic anisotropy in an AFM-coupled Fe(III) dimer, taking advantage of the diamagnetic substitution method. The anisotropy arises predominantly from single-ion ZFS terms and, to a lesser extent, from spin–spin interactions. From the analysis of the anisotropic spin–spin interaction tensor, we have demonstrated that the exchange (through-bond) interaction contributes an anisotropic part which is of comparable magnitude to the dipolar (through-space) interaction, and even to the rhombic part of the single-ion ZFS. We argue that anisotropic exchange contributions cannot in principle be excluded in the case of larger cluster compounds, such as the Fe4 or Fe8 single-molecule magnets or the antiferromagnetic iron wheels, which are based on similar exchange couplings between Fe(III) ions.

4. Experimental

4.1. Synthesis

Methanol and chloroform were carefully dried by treatment with Mg/I_2 and $CaCl_2$, respectively, and distilled before use. All other chemicals were reagent grade and were used as received. A 2.96-M solution of $NaOCH_3$

was prepared by careful addition of sodium metal to anhydrous methanol. Single crystals of Fe2 suitable for EPR studies were prepared by a modification of the procedure reported [33]. Iron wire (99.99%, 0.335 g, 6.00 mmol) was dissolved in 2.5 mL aqua regia [HCl(conc)/HNO_3(conc) 3:1 v/v]. The solution was evaporated almost to dryness under heating and treated with 0.5 mL HCl(conc). The procedure was repeated once and a final evaporation until incipient precipitation was performed. Treatment of the residue with several 1-mL portions of $SOCl_2$ followed by removal of excess $SOCl_2$ by distillation under nitrogen afforded a lustrous black solid ($FeCl_3$). The latter was dissolved in methanol to a final volume of 50 mL (0.120 M). A solution of Hdbm (1.077 g, 4.80 mmol) and $NaOCH_3$ (3.04 mL, 9.00 mmol) in methanol (60 mL) was added dropwise over a 30′-period to the above-mentioned $FeCl_3$ solution (20.0 mL, 2.40 mmol). After 15′ stirring, the orange precipitate was collected by filtration and dried under vacuum (1.10 g, 86%). The solid was dissolved in $CHCl_3$ (14 mg/mL) and the filtered solution was layered with an equal volume of methanol. The air-stable red prisms of Fe2, obtained in one week, had the same unit cell reported in [33]. Air-stable, iron(III)-doped crystals of Ga2 (2 Fe mol%) were grown as described in [27]. The resulting single crystals were of dimensions adequate for the W-band EPR studies, i.e., approximately $0.5 \times 0.5 \times 0.1$ mm^3 (platelets) for doped Ga2 and $0.7 \times 0.7 \times 0.7$ mm^3 (prismatic) for Fe2.

The EPR experiments were performed using a continuous wave W-band EPR spectrometer (Bruker ElexSys E680), with a cylindrical cavity operating at 94 GHz and a split coil superconducting magnet (Oxford) of 6 T. The system was equipped with a continuous flow cryostat operating from room temperature down to 4.2 K. The sample holder could be rotated around a vertical axis with a precision of 0.5° to 1° for measurements of doped Ga2, using a normal goniometer, and of 0.1° for measurements on Fe2, using an angle encoder with digital read-out.

For the description of the experiments and of the interaction matrices in the spin Hamiltonian, we define an orthogonal reference frame (xyz) attached to the crystal, with $x//a$, z perpendicular to x in the ac-plane, and y perpendicular to x and z. With this choice, the xz-plane coincides with the crystallographic ac-plane, which was one of the planes of measurement. Furthermore, the angle between a and c is 88°, so z is almost parallel to c.

Oriented single crystals of both compounds were mounted on polished silica rods of 0.84 mm diameter [32], guided by the outer morphology with facets that were indexed by X-ray diffraction. In the case of the iron doped Ga2 single crystals, the angular dependences could be recorded in the three mutually orthogonal planes: $xz = ac$, with the platelet mounted flat on the end of the quartz rod, and xy and yz with the platelet flat on a vertical plane polished on the side of the quartz rod. In the case of Fe2, the measurements had to be performed in the crystalline planes ac, bc, and ab, with the corresponding outer plane of the prismatic sample flat on the bottom of the quartz rod. Errors in the plane orientation of the order of 5° can be expected due to the visual mounting procedure under a microscope. One additional plane was also studied in the Fe2 crystal, containing the crystal axis a, as well as the Fe–Fe vector as derived from the crystallographic data. The latter sample was oriented using a 4-circle X-ray diffractometer and a home-made device for direct transfer to a W-band quartz sample tube on which it was glued, yielding an estimated orientational accuracy of 0.5°.

The analysis of the spectra was performed with the dedicated simulation and fitting programs "SIM" [41,42] and "ESRFIT" [43], developed by Prof. H. Weihe of the Department of Chemistry, University of Copenhagen. To reach the best fit of the angular dependences in the different planes, allowance was made for deviations from the nominal plane by rotations of the order of the estimated alignment errors. This procedure was not applied for the a–Fe–Fe plane which has been very accurately oriented.

Acknowledgments

One of us (P.t.H.) thanks the Flemish science supporting agency IWT for a scholarship. Financial support from the Fund for Scientific Research (FWO-Vlaanderen, programme G.0409.02N) is gratefully acknowledged.

Appendix A. Supplementary data

Supplementary data associated with this article can be found, in the online version, at doi:10.1016/j.jmr.2005.10.016.

References

[1] O. Kahn, Molecular Crystals and Liquid Crystals, Wiley-VCH, 1993.
[2] D. Gatteschi, R. Sessoli, J. Magn. Magn. Mater. 272–276 (2004) 1030–1036.
[3] J.R. Long, in: P. Yang (Ed.), Chemistry of Nanostructured Materials, World Scientific Publishing, Hong Kong, 2003, pp. 291–315.
[4] S.J. Blundell, F.L. Pratt, J. Phys.-Condens. Mat. 16 (2004) R771–R828.
[5] A.L. Barra, D. Gatteschi, R. Sessoli, Chem.-Eur. J. 6 (2000) 1608–1614.
[6] M. Bal, J.R. Friedman, Y. Suzuki, K.M. Mertes, E.M. Rumberger, D.N. Hendrickson, N. Avraham, Y. Myasoedov, H. Shtrickman, E. Zeldov, Phys. Rev. B 70 (2004) 100408.
[7] A.K. Boudialis, B. Donnadieu, V. Nastopoulos, J.M. Clemente-Juan, A. Mari, Y. Sanakis, J.-P. Perlepes, Angew. Chem. 116 (2004) 2316–2320.
[8] A. Cornia, A.C. Fabretti, P. Garrisi, C. Mortalo, D. Bonacchi, D. Gatteschi, R. Sessoli, L. Sorace, W. Wernsdorfer, A.-L. Barra, Angew. Chem. Int. Ed. 43 (2004) 1136–1139.
[9] E.K. Brechin, E.C. Sanudo, W. Wernsdorfer, C. Boskovic, J. Yoo, D.N. Hendrickson, A. Yamaguchi, H. Ishimoto, T.E.T.E. Concolino, A.L. Rheingold, G. Christou, Inorg. Chem. 44 (2005) 502–511.
[10] M. Soler, W. Wernsdorfer, K.A. Abboud, D.N. Hendrickson, G. Christou, Polyhedron 22 (2003) 1777–1782.
[11] E. Del Barco, A.D. Kent, E.C. Yang, D.N. Hendrickson, Phys. Rev. Lett. 93 (2004) 157202.

[12] E.C. Yang, W. Wernsdorfer, S. Hill, R.S. Edwards, M. Nakano, S. Maccaqnano, L.N. Zakharov, A.L. Rheingold, G. Christou, D.N. Hendrickson, Polyhedron 22 (2003) 1727–1733.
[13] E.C. Yang, D.N. Hendrickson, W. Wernsdorfer, M. Nahano, L.N. Zakhorov, R.D. Sommer, A.L. Rheingold, J. Appl. Phys. 91 (2002) 7382–7384.
[14] B. Barbara, L. Gunther, Phys. World 12 (1999) 35–39.
[15] A. Caneschi, D. Gatteschi, R. Sessoli, RICHMAC Mag. 80 (1998) 1317–1322.
[16] G. Christou, D. Gatteschi, D.N. Hendrickson, R. Sessoli, MRS Bull. 25 (2000) 66–71.
[17] A.L. Barra, A. Caneschi, A. Cornia, F. Fabrizi de Biani, D. Gatteschi, C. Sangregorio, R. Sessoli, L. Sorace, J. Am. Chem. Soc. 121 (1999) 5302–5310.
[18] D. Gatteschi, R. Sessoli, Angew. Chem. Int. Ed. 3 (2003) 268–297.
[19] A.L. Barra, D. Gatteschi, R. Sessoli, Phys. Rev. B 56 (1997) 8192–8198.
[20] A.L. Barra, F. Bencini, A. Caneschi, D. Gatteschi, C. Paulsen, R. Sessoli, L. Sorace, ChemPhysChem 2 (2001) 523–531.
[21] M. Dressel, B. Gorshunov, K. Rajagopal, S. Vongtragool, A.A. Mukhin, Phys. Rev. B 67 (2003) 060405.
[22] A.L. Barra, L.-C. Brunel, D. Gatteschi, L. Pardi, R. Sessoli, Accounts Chem. Res. 31 (1998) 460–466.
[23] M.N. Leuenberger, D. Loss, Nature 410 (2001) 789–793.
[24] (a) B. Normand, X. Wang, X. Zotos, D. Loss, Phys. Rev. B 63 (2001) 184409;
(b) F. Troiani, A. Ghirri, M. Affronte, S. Carretta, P. Santini, G. Amoretti, S. Piligkos, G. Timco, R.E.P. Winpenny, Phys. Rev. Lett. 94 (2005) 207208.
[25] O. Cador, D. Gatteschi, R. Sessoli, F.K. Larsen, J. Overgaard, A.-L. Barra, S.J. Teat, G.A. Timco, R.E.P. Winpenny, Angew. Chem. Int. Ed. 43 (2004) 5046.
[26] J. van Slageren, R. Sessoli, D. Gatteschi, A.A. Smith, M. Helliwell, R.E.P. Winpenny, A. Cornia, A.-L. Barra, A.G.M. Jansen, E. Rentschler, G.A. Timco, Chem.-Eur. J. 8 (2002) 277–285.
[27] G.L. Abbati, L.-C. Brunel, H. Casalta, A. Cornia, A.C. Fabretti, D. Gatteschi, A. Hassan, A.G.M. Jansen, A.L. Maniero, L. Pardi, C. Paulsen, U. Segre, Chem.-Eur. J. 7 (2001) 1796–1807.
[28] A. Bouwen, A. Caneschi, D. Gatteschi, E. Goovaerts, D. Schoemaker, L. Sorace, M. Stefan, J. Phys. Chem. B 105 (2001) 2658–2663.
[29] A. Cornia, D. Gatteschi, R. Sessoli, Coordin. Chem. Rev. 219-221 (2001) 573–604.
[30] A. Ozarowski, B.R. McGarvey, J.E. Drake, Inorg. Chem. 34 (1995) 5558–5566.
[31] A. Caneschi, A. Dei, D. Gatteschi, C.A. Massa, L.A. Pardi, S. Poussereau, L. Sorace, Chem. Phys. Lett. 371 (2003) 694–699.
[32] J.A. Weil, J.R. Bolton, J.E. Wertz, Electron Paramagnetic Resonance—Elementary Theory and Practical Applications, Wiley, New York, 1994.
[33] F. Le Gall, F.F. de Biani, A. Caneschi, P. Cinelli, A. Cornia, A.C. Fabretti, D. Gatteschi, Inorg. Chim. Acta 262 (1997) 123–132.
[34] A. Bencini, D. Gatteschi, EPR of Exchange Coupled Systems, Springer-Verlag, Berlin, 1990 (Chapter 3).
[35] (a) E. Liviotti, S. Carretta, G. Amoretti, J. Chem. Phys. 114 (2002) 3361–3368;
(b) S. Carretta, E. Liviotti, N. Magnani, P. Santini, G. Amoretti, Phys. Rev. Lett. 92 (2004) 207205.
[36] D. Collison, D.M.L. Goodgame, M.A. Hitchman, B. Lippert, F.E. Mabbs, E.J.L. McInnes, Inorg. Chem. 41 (2002) 2826–2833.
[37] D. Gatteschi, L. Sorace, J. Solid State Chem. 159 (2001) 253–261.
[38] T.E. Machonkin, P. Mukherjee, M.J. Henson, T.D.P. Stack, E.I. Solomon, Inorg. Chim. Acta 341 (2002) 39–44.
[39] P.K. Ross, M.D. Allendorf, E.I. Solomon, J. Am. Chem. Soc. 111 (1989) 4009–4021.
[40] L. Banci, A. Bencini, D. Gatteschi, J. Am. Chem. Soc. 105 (1983) 761–764.
[41] J. Glerup, H. Weihe, Acta Chem. Scand. 45 (1991) 444–448.
[42] C.J. Jacobsen, E. Pedersen, J. Villadsen, H. Weihe, Inorg. Chem. 32 (1993) 1216–1221.
[43] S. Mossin, M. Stefan, P. ter Heerdt, A. Bouwen, E. Goovaerts, H. Weihe, Appl. Magn. Reson. 21 (2001) 587–596.